Preprints, 4th IFAC Conference on
Advances in Proportional-Integral-Derivative Control
Almería, Spain | June 12-14, 2024

A Nonlinear Integrator Based on the First-Order Reset Element ⋆

Luke F. van Eijk [*,**] **Yixuan Liu** [*,***] **Xinxin Zhang** [*]
Dragan Kostić [**] **S. Hassan HosseinNia** [*]

[*] *Department of Precision and Microsystems Engineering, Delft University of Technology, 2628 CD Delft, The Netherlands (e-mail: {L.F.vanEijk, X.Zhang-15, S.H.HosseinNiaKani}@tudelft.nl).*
[**] *ASMPT, 6641 TL Beuningen, The Netherlands (e-mail: dragan.kostic@asmpt.com).*
[***] *Delft Center for Systems and Control, Delft University of Technology, 2628 CD Delft, The Netherlands (e-mail: Y.Liu-24@tudelft.nl).*

Abstract: This work proposes a novel nonlinear Proportional-Integral (PI) controller, which utilizes a generalized first-order reset element. The proposed element can achieve similar magnitude-characteristics as its linear counterpart but with less phase lag at the open-loop crossover frequency (i.e. the control bandwidth), according to a sinusoidal-input describing function (SIDF) analysis. The same can be achieved with an existing reset-based integrator, the Clegg integrator (CI). However, it is known that a Proportional-CI (PCI) element can excessively generate higher-order harmonics of its input, which are neglected in the SIDF-analysis. Furthermore, a PCI can cause a limit cycle when placed in closed-loop with certain types of plants. The novel PI controller proposed in this work can prevent the limit cycle and can reduce the generation of higher-order harmonics, while retaining the beneficial phase advantage that is associated with existing reset-based PI controllers.

Keywords: PI control, nonlinear feedback control, reset control, limit cycle, higher-order harmonics, frequency-domain

1. INTRODUCTION

Linear control has been an important factor in enabling and improving numerous industrial applications, ranging from chemical process plants to semiconductor chip manufacturing equipment (Lamnabhi-Lagarrigue et al., 2017). Proportional-Integral-Derivative (PID) feedback controllers are conventionally utilized, among others because they are relatively easy to implement and design (Åström and Hägglund, 2001). The latter can be done in the frequency-domain using a frequency-response function (FRF) of the plant, which can be acquired based solely on measurement data. However, linear control is subject to inherent limitations, which can for example be characterised by means of Bode's gain-phase relationship or trade-offs between overshoot and rise-time specifications (Freudenberg et al., 2000).

Reset control is a nonlinear control technique that can overcome certain limitations of linear control, as illustrated by e.g. Beker et al. (2001). The first reset element was developed by Clegg (1958), which is known as the Clegg integrator (CI). This element behaves like a linear integrator but resets its output to zero when the input signal is equal to zero. In Clegg (1958), a sinusoidal-input describing function (SIDF) analysis of the CI was performed, which suggests that the element can overcome Bode's gain-phase relationship. In a SIDF-analysis, the CI's output behaviour is investigated when excited with a sinusoidal input. Although the output signal is not sinusoidal, the SIDF-analysis investigates the behaviour of the first-order harmonic, i.e. the harmonic with the same frequency as the input signal. This first-order harmonic shows equivalent magnitude-characteristics as a linear integrator. However, whereas a linear integrator has a phase lag of 90°, this is only 38.1° for the CI.

Even though a SIDF-analysis illustrates that the CI has potential for replacing the integral part of the classical (linear) PID element, it can also introduce certain problems. First, the CI can excite high-frequent resonances of the plant that is being controlled. Namely, while neglected by the SIDF-analysis, the CI's output signal also contains higher-order harmonics of its input signal (Saikumar et al., 2021). Since these higher-order harmonics are injected into the plant, they can excite resonances in the overlapping frequency-ranges. Second, the CI can cause a limit cycle in the closed-loop system (HosseinNia et al., 2014). Since these problems are already observable when utilizing a more simple PI element, we will focus on that control configuration in this work.

There exist several nonlinear alternatives for the CI element which tackle one or both of the described problems. However, in this work we are only interested in reset elements that (partially) reset their state(s) when

⋆ This work is supported by ASMPT.

the input signal is zero. Namely, this is the only class of nonlinear elements for which control design tools have been developed that only rely on a plant FRF and are able to capture the effect of higher-order harmonics generation on the closed-loop system (Saikumar et al., 2021). One control structure exists that: (1) fits into this class of reset elements, (2) can reduce the generation of higher-order harmonics, and (3) can prevent the limit cycle. This so-called PI+CI element has been developed by Baños and Vidal (2007), which contains both a linear integrator and a CI, both taking a fraction of the total integral action. However, reducing the higher-order harmonics simply means that a larger fraction of the integral action is taken by the linear integrator. Therefore, reducing the problem inherently means trading off the benefit the CI element offers, i.e. its phase advantage.

In this work we propose a novel reset integrator that can mitigate negative impact of higher-order harmonics and can prevent the limit cycle, without trading off the beneficial phase advantage associated with the CI element. In order to achieve this, a key insight is that phase advantage is often only required around the control bandwidth, in order to achieve sufficient phase margin. To develop the proposed integrator, inspiration is taken from Heertjes et al. (2021); Hosseini et al. (2022); van Eijk et al. (2023), where another nonlinear integrator strategy is developed based on the hybrid integrator-gain system (HIGS). In this work we use a similar approach but make use of a generalized first-order reset element (GFORE) instead of HIGS, which have a similar SIDF. The benefit of using a GFORE is that its phase lag – according to a SIDF-analysis – can be tuned between $-90°$ and $0°$, while with HIGS it is only possible to achieve a phase lag between $-90°$ and $-38.15°$. Furthermore, it is unclear how the higher-order harmonics generated by HIGS affect the closed-loop system, while these effects can be analysed for our proposed (reset-based) integrator using the tools in Saikumar et al. (2021).

The remainder of this paper is organized as follows. In Section 2 the necessary theoretical preliminaries are given. We propose our novel integrator in Section 3. Its benefits in terms of reducing higher-order harmonics generation and preventing the limit cycle are discussed in Section 4 and 5, respectively. Finally, Section 6 provides concluding remarks and elaborates on future research.

2. PRELIMINARIES

Consider the reset element given in state-space representation by

$$R := \begin{cases} \dot{x}(t) = \omega_{\mathrm{r}}\big(e(t) - bx(t)\big), & \text{if } e(t) \neq 0, \\ x(t^+) = \gamma x(t), & \text{if } e(t) = 0, \\ v(t) = x(t), \end{cases} \tag{1}$$

with state $x \in \mathbb{R}$, input $e \in \mathbb{R}$, output $v \in \mathbb{R}$, integrator frequency $\omega_{\mathrm{r}} \in \mathbb{R}_{>0}$, reset fraction $\gamma \in (-1, 1]$, $b \in \{0, 1\}$, and time $t \in \mathbb{R}$, where $t^+ := \lim_{\tau \to t+0} \tau$. By setting $b = 0$ and $\gamma = 0$, the CI is obtained (Clegg, 1958). As part of our proposed integrator we utilize a GFORE, which is obtained by setting $b = 1$ (Saikumar et al., 2021).

To analyse the frequency-domain behaviour of the reset element, we can perform a higher-order SIDF (HOSIDF) analysis, as developed by Nuij et al. (2006). In this method,

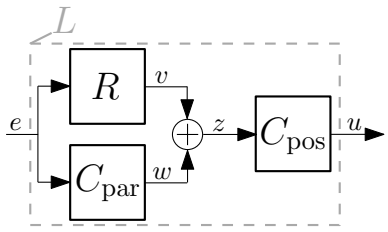

Fig. 1. Schematic representation of a system L with reset element R and LTI elements C_{par} and C_{pos}.

we consider the response to sinusoidal inputs $e(t) = \hat{e}\sin(\omega t)$, with amplitude $\hat{e} \in \mathbb{R}_{>0}$ and frequency $\omega \in \mathbb{R}_{>0}$. For these inputs, the output of the reset element converges to a $\frac{2\pi}{\omega}$-periodic solution (Guo et al., 2009, Proposition 2). Therefore, according to Saikumar et al. (2021), this stationary output can be described by the Fourier series

$$v_{\mathrm{s}}(t) = \sum_{n=1}^{\infty} |H_n(\omega)|\hat{e}\sin\big(n\omega t + \angle H_n(\omega)\big), \tag{2}$$

where $H_n \in \mathbb{C}$ is the n^{th}-order SIDF, with order $n \in \mathbb{N}$. An analytical expression for the HOSIDFs of the reset element has been derived in Saikumar et al. (2021). For later use, a special case of Saikumar et al. (2021) is given in Lemma 1, which contains an analytical expression for the HOSIDFs of a GFORE.

Lemma 1. (Saikumar et al., 2021, Theorem 3.1) The HOSIDFs of a GFORE, i.e. reset element R with $b = 1$, are given by

$$H_n(\omega) := \begin{cases} \omega_{\mathrm{r}}(\omega_{\mathrm{r}} + j\omega)^{-1}\big(1 + j\Theta_{\mathrm{D}}(\omega)\big), & \text{for } n = 1, \\ \omega_{\mathrm{r}}(\omega_{\mathrm{r}} + jn\omega)^{-1} j\Theta_{\mathrm{D}}(\omega), & \text{for odd } n \geq 2, \\ 0, & \text{for even } n, \end{cases} \tag{3}$$

where $j := \sqrt{-1}$ and

$$\Theta_{\mathrm{D}}(\omega) = \frac{2(1-\gamma)}{\pi} \cdot \frac{\omega^2}{\omega^2 + \omega_{\mathrm{r}}^2} \cdot \frac{1 + \mathrm{e}^{(-\pi\omega_{\mathrm{r}}/\omega)}}{1 + \gamma\mathrm{e}^{(-\pi\omega_{\mathrm{r}}/\omega)}}. \tag{4}$$

Since our proposed integrator also considers linear time-invariant (LTI) control elements in parallel and after the GFORE, consider the system L shown in Fig. 1. This system consists of reset element R, LTI element C_{par} with output $w \in \mathbb{R}$, and LTI element C_{pos} with input $z := v + w$ and output $u \in \mathbb{R}$. Note that the input-output relations of C_{par} and C_{pos} can be described in the frequency-domain by $W(s) = C_{\mathrm{par}}(s)E(s)$ and $U(s) = C_{\mathrm{pos}}(s)Z(s)$, respectively. Here, $s \in \mathbb{C}$ is the Laplace variable, and the capitalized variables $E, W, Z, U \in \mathbb{C}$ are the Laplace transforms of the respective non-capitalized time-domain signals. The HOSIDFs of the complete system L are given by (Karbasizadeh, 2023, Chapter 10)

$$L_n(\omega) := \begin{cases} C_{\mathrm{pos}}(j\omega)\left[H_1(\omega) + C_{\mathrm{par}}(j\omega)\right], & \text{for } n = 1, \\ C_{\mathrm{pos}}(nj\omega)H_n(\omega), & \text{for odd } n > 1, \\ 0, & \text{for even } n, \end{cases} \tag{5}$$

where the even-order SIDFs are zero because the even-order SIDFs of the reset element are zero (Saikumar et al., 2021, Theorem 3.1).

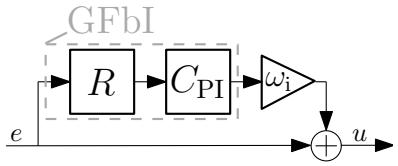

Fig. 2. Schematic representation of the proposed nonlinear PI element, with a GFORE in reset element R ($b = 1$) and LTI element C_{PI}.

3. DEFINITION OF NOVEL PI-ELEMENT

Consider an LTI PI-element, given in the frequency-domain by

$$C_{\mathrm{lin}}(s) = 1 + \omega_{\mathrm{i}} \cdot \frac{1}{s}, \tag{6}$$

with integrator frequency $\omega_{\mathrm{i}} \in \mathbb{R}_{\geq 0}$. We propose the nonlinear PI-element shown in Fig. 2, where the linear integrator is replaced by a series connection of a GFORE and another LTI PI element, given in the frequency-domain by

$$C_{\mathrm{PI}}(s) = \frac{\omega_{\mathrm{c}} + s}{\omega_{\mathrm{c}} s}, \tag{7}$$

with phase-shift frequency $\omega_{\mathrm{c}} \in \mathbb{R}_{>0}$. Subsequently, the GFORE's integrator frequency is fixed as

$$\omega_{\mathrm{r}} = \frac{\omega_{\mathrm{c}}}{\sqrt{1 + \Theta_{\mathrm{D},\infty}^2}}, \quad \Theta_{\mathrm{D},\infty} = \frac{4(1-\gamma)}{\pi(1+\gamma)}. \tag{8}$$

Hereby, the SIDF of this GFORE-based integrator (GFbI) has equivalent magnitude-characteristics as an LTI integrator

$$C_{\mathrm{int}}(s) = \frac{1}{s}, \tag{9}$$

for the low-frequent ($\omega \to 0$) and high-frequent ($\omega \to \infty$) limit cases (see Appendix A for proofs). This is portrayed in Fig. 3, which provides the magnitude- and phase-characteristics of a GFbI's SIDF, as well as the elements constructing it, and compares it to LTI integrator C_{int}. Note that the GFbI's SIDF can be constructed using (5) by substituting $C_{\mathrm{par}}(s) = 0$ and $C_{\mathrm{pos}}(s) = C_{\mathrm{PI}}(s)$. The figure shows that the magnitude-characteristics of the GFbI's SIDF are similar to those of the LTI integrator over the complete frequency-range. However, a difference can be observed in terms of the phase-characteristics. The LTI integrator has a phase lag of 90° over the complete frequency-range. While this is also the case for the GFbI in the low-frequency range, the phase lag reduces in the high-frequency range.

The frequency at which the phase changes can be tuned using phase-shift frequency ω_{c}, as visualized in Fig. 4a. For frequencies lower than ω_{c} the GFbI behaves like an LTI integrator, whereas for frequencies higher than ω_{c} it behaves like a generalized CI (GCI) – a CI with nonzero reset fraction γ – with

$$\omega_{\mathrm{r}} = \frac{1}{\sqrt{1 + \Theta_{\mathrm{D},\infty}^2}}. \tag{10}$$

Namely, when tuning the GCI's integrator frequency according to this relation, its SIDF has equivalent magnitude-characteristics as LTI integrator C_{int} over the complete frequency-range (Guo et al., 2009).

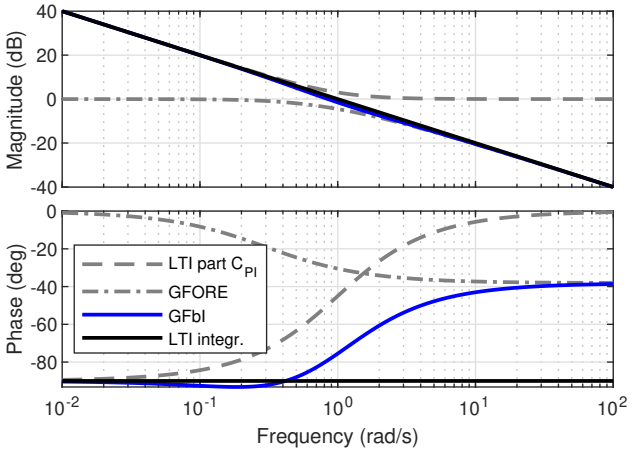

Fig. 3. Magnitude- and phase-characteristics of LTI element C_{PI} ($\omega_{\mathrm{c}} = 1$), the SIDF of a GFORE ($\gamma = 0$) with ω_{r} as in (8), and the SIDF of their series connection, compared with LTI integrator C_{int}.

Apart from tuning the frequency-range in which the SIDF shows reduced phase lag, a specific phase can be obtained at the high-frequent limit-case by tuning reset fraction γ according to the relationship (Guo et al., 2009)

$$\lim_{\omega \to \infty} \angle L_1(\omega) = \arctan\left(\frac{4(1-\gamma)}{\pi(1+\gamma)}\right) - \frac{\pi}{2}. \tag{11}$$

Note that the phase is completely determined by the GFORE, because the phase of LTI element C_{PI} converges to 0°. The result for various reset fractions is visualized in Fig. 4b. One can observe from the figure that the SIDF is equivalent to that of LTI integrator C_{int} when reset fraction $\gamma = 1$, since this means that no reset happens at all. When decreasing the reset fraction, the phase lag reduces. Eventually, for $\gamma \to -1$, the phase even approaches 0°. In conclusion we can observe that the level of phase lag reduction, as well as the frequency-range in which this occurs, can be tuned independently from the magnitude-characteristics.

Remark 2. The possibility of tuning the GFbI's phase in the high-frequency range, shows similarities to what can be done using an LTI fractional integrator. However, note that the SIDF-based magnitude- and phase-characteristics of a GFbI are not constrained by Bode's gain-phase relationship. Therefore, these characteristics cannot be achieved using any LTI system, even if they are of fractional-order.

4. REDUCTION OF HIGHER-ORDER HARMONICS

From the point of view of a SIDF-analysis, the most beneficial phase-characteristics of the GFbI would be obtained if $\omega_{\mathrm{c}} \to 0$, which means that the GFbI reduces to a GCI. When $\gamma \to -1$, it is even possible to achieve no phase lag over the complete frequency-range. However, a SIDF-analysis neglects the higher-order harmonics that are generated by the GFbI. When the magnitude of the HOSIDFs is reduced compared to the magnitude of the SIDF, this means that a SIDF-analysis becomes more accurate.

As explained earlier, the HOSIDFs of a GFbI can be derived using (5). In the remainder we will analyse the

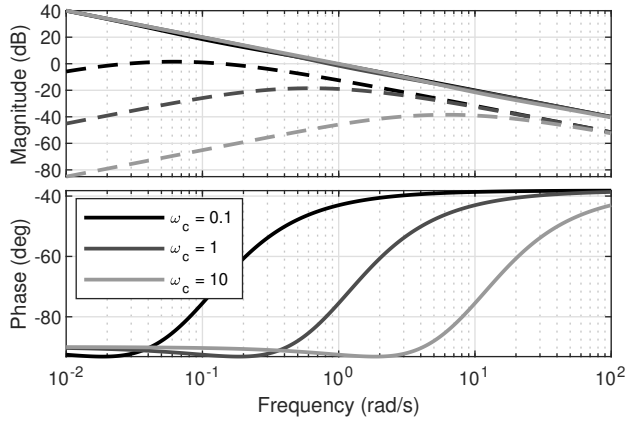

(a) Varying ω_c and $\gamma = 0$.

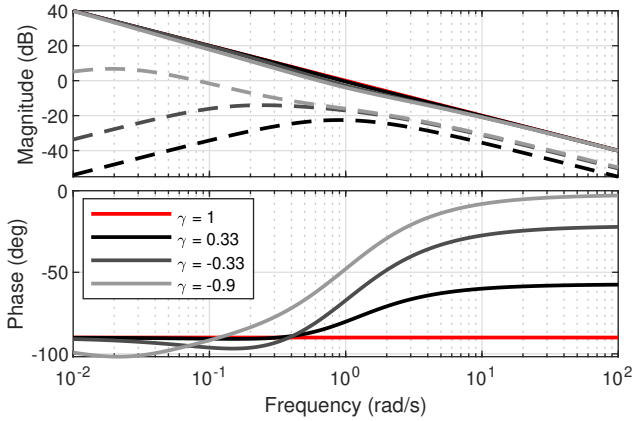

(b) Varying γ and $\omega_c = 1$.

Fig. 4. Magnitude- and phase-characteristics for the first- and third-order SIDF of a GFbI.

higher-order harmonics by focusing on the magnitude-characteristics of the third-order SIDF. Namely, on one hand, the even-order SIDFs are all equal to zero, because the even-order SIDFs of a GFORE are equal to zero (see Lemma 1). On the other hand, a GFORE's odd-order SIDFs with $n > 3$ always have a lower magnitude than the third-order SIDF. Namely, according to Lemma 1, its magnitude-characteristics are given by

$$|H_n(\omega)| = \frac{\omega_r \Theta_{\mathrm{D}}(\omega)}{\sqrt{\omega_{\mathrm{r}}^2 + n^2\omega^2}}. \tag{12}$$

For any frequency ω, a larger n results in a lower magnitude of the HOSIDF. Since the goal is to keep the magnitudes of all HOSIDFs small compared to the SIDF, such that they can be neglected, designing a low third-order SIDF directly means that all HOSIDFs are at least as low as that one. For the same reason, the phase-characteristics of the HOSIDFs will not be further analyzed.

In Fig. 4a, the magnitude-characteristics of the GFbI's third-order SIDF are visualized for different values of phase-shift frequency ω_c. As concluded earlier, increasing ω_c results in a smaller frequency-range with reduced phase lag. However, one can also observe that increasing ω_c results in smaller HOSIDFs, especially for frequencies lower than ω_c. For frequencies higher than ω_c, the magnitude of the third-order SIDF is similar and almost independent from ω_c. To lower the magnitude of the third-order SIDF for frequencies higher than ω_c, one can tune reset fraction

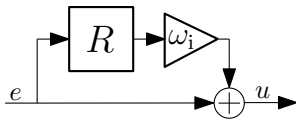

Fig. 5. Schematic representation of a PCI-element, with a CI in R ($b = 0$, $\gamma = 0$) and ω_{r} as in (10).

γ, as displayed in Fig. 4b. By increasing the reset fraction, the magnitude of the third-order SIDF is decreased over the complete frequency-range. For $\gamma = 1$, i.e. an LTI integrator, the magnitude of the third-order SIDF is equal to zero.

The benefit of the GFbI over the CI, in terms of higher-order harmonics reduction, becomes apparent when studying it as a part of the proposed nonlinear PI-element. Therefore, we compare our proposed structure shown in Fig. 2 with the PCI-element displayed in Fig. 5. By presenting both systems in a different manner, its HOSIDFs can still be computed using (5). Namely, the system shown in Fig. 2 is equivalent to the system in Fig. 1 when choosing $C_{\mathrm{pos}}(s) = \omega_{\mathrm{i}} C_{\mathrm{PI}}(s)$ and $C_{\mathrm{par}}(s) = \frac{1}{\omega_{\mathrm{i}} C_{\mathrm{PI}}(s)}$. The same holds for the system shown in Fig. 5 by choosing $C_{\mathrm{pos}}(s) = \omega_{\mathrm{i}}$ and $C_{\mathrm{par}}(s) = \frac{1}{\omega_{\mathrm{i}}}$.

The magnitude- and phase-characteristics of a PCI's first- and third-order SIDF are visualized in Fig. 6. One can observe that the difference in magnitude between the first- and third-order SIDF is large in the high-frequency range. However, in the low-frequency range the magnitude-gap is only 11.6 dB. Even though the first-order SIDF is still dominant, the influence of higher-order harmonics cannot be neglected. Next, consider our proposed PI-element with the same integrator frequency ω_{i}, $\omega_c = 0.9$, and $\gamma = -0.5$, for which the magnitude- and phase-characteristics of the first- and third-order SIDF are also portrayed in Fig. 6. One can observe that the proposed PI-element not only yields a large magnitude-gap in the high-frequency range, but also in the low-frequency range. Furthermore, the smallest magnitude gap can be observed at a frequency of $\omega = 0.593$, which is equal to 18.74 dB. Therefore, the magnitude gap of the proposed PI-element is, for all frequencies, larger than the smallest gap with the PCI. Even though the HOSIDFs of the proposed PI-element are overall reduced compared to the PCI, it is able to achieve better first-order SIDF phase-characteristics. Namely, consider the case in which both nonlinear PI elements are utilized to control a plant. The frequency at which the open-loop FRF has a magnitude of 0 dB – the control bandwidth – is often chosen to be larger than the integrator cut-off frequency ω_{i} (Munnig Schmidt et al., 2014). In this example, the phase advantage of our proposed element is larger than the one of the PCI for frequencies $\omega > 1.4\omega_{\mathrm{i}}$. Specifically at $\omega = 5\omega_{\mathrm{i}}$, our proposed PI-element yields 1.6° less phase lag than the PCI element. By further utilizing this benefit, one can also increase the integrator frequency ω_{i} to achieve a larger low-frequent magnitude. This is also visualized in Fig. 6, showing that we can achieve a 5.6 dB larger magnitude in the low-frequency range, while having the same phase lag as the PCI at $\omega = 5\omega_{\mathrm{i}}$, as well as a larger magnitude gap (16.48 dB) between the first- and third-order SIDF.

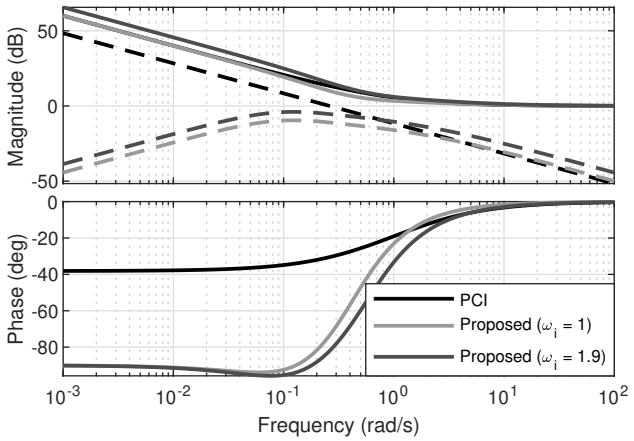

Fig. 6. Magnitude- and phase-characteristics for the first-order (solid) and third-order (dashed) SIDF of a PCI ($\omega_\mathrm{i} = 1$), compared to the proposed PI-element with $\omega_\mathrm{c} = 0.9$, $\gamma = -0.5$, and $\omega_\mathrm{i} \in \{1, 1.908\}$.

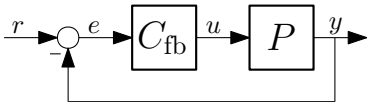

Fig. 7. Schematic representation of a closed-loop system with LTI plant P and feedback controller C_fb.

Remark 3. Instead of comparing the proposed PI to a PCI, we could have also chosen other reset-based elements, such as a PI+CI or one containing a GCI. However, with both of these it remains impossible to achieve less phase lag and a larger magnitude gap between the first- and third-order SIDF at the same time.

5. LIMIT CYCLE PREVENTION

In this section we show that the proposed PI-element can prevent the undesired limit cycle which can arise with a PCI, when these are utilized to control certain types of plants. For that purpose, consider the closed-loop system shown in Fig. 7, consisting of an LTI plant P with output $y \in \mathbb{R}$ and input u, and feedback controller C_fb with output u and input $e := r - y$, where $r \in \mathbb{R}$ is the reference signal.

Consider a simple first-order plant, given in the frequency-domain by

$$P(s) = \frac{0.1}{s + 0.1}, \tag{13}$$

which already suffices to illustrate the occurrence of the limit cycle. Consider the case in which the plant is controlled by the LTI PI-element in (6), where $\omega_\mathrm{i} = 1.3917$ is tuned to achieve a phase margin of 30°. The step response that is obtained with this feedback controller is portrayed in Fig. 8. One can observe that, after the initial rise time, the system overshoots the reference and oscillates around the reference until it settles. Next, we replace the LTI PI-element for a PCI with the same integrator frequency ω_i. The step response shows that the overshoot can be eliminated. However, the system suffers from the limit cycle (HosseinNia et al., 2014). Namely, each time when the reference position is reached, i.e. the error signal is equal to zero, the state of the integrator is reset to zero. Hence, the control output that is necessary

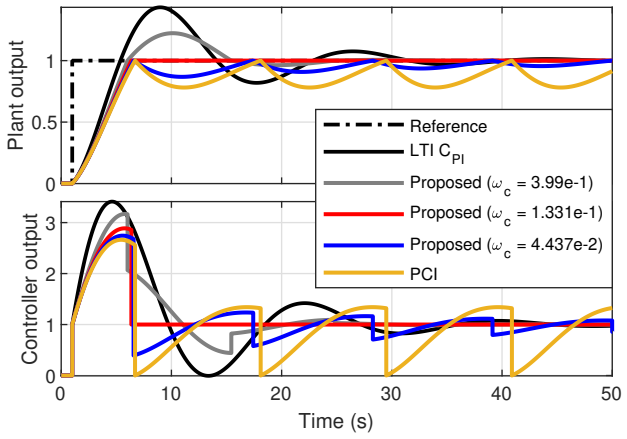

Fig. 8. Numerical step response simulations with plant P in (13), controlled by either LTI PI C_lin, a PCI, or a proposed PI-element ($\gamma = 0$, $\omega_\mathrm{c} \in \{0.399, 0.1331, 0.04437\}$), all with $\omega_\mathrm{i} = 1.3917$.

to stay in the equilibrium is removed, and the system will show undershooting behaviour. This cycle will then continue to repeat itself. To prevent the limit cycle, our proposed nonlinear PI-element can be utilized. By tuning the phase-shift frequency ω_c, one can tune the behaviour between that of the LTI PI-element ($\omega_\mathrm{c} \to \infty$) and the PCI-element ($\omega_\mathrm{c} \to 0$). When starting with a high value for the phase-shift frequency, reducing it will lower the overshoot caused by the LTI PI-element and allows for faster settling. When starting with a low value, increasing it will diminish the undershoot caused by the PCI-element. Furthermore, the undershoot is not persistent anymore. Namely, our proposed solution internally incorporates an LTI PI-element after the GFORE, which makes it possible to build and retain the control output that is necessary to stay at the reference. Finally, it is interesting to see that – by properly tuning the phase-shift frequency – it is possible to achieve neither overshoot nor undershoot. After the initial rise time, the system will instantly settle at the reference.

Remark 4. Note that step response simulations with the plant in (13) have also been performed in Baños and Vidal (2007), where instead a PI+CI element was utilized to prevent the limit cycle. By properly tuning its fraction of nonlinear versus linear integral action, it is also possible to achieve finite-time convergence without any overshoot (Nair et al., 2018). A benefit of our proposed PI-element is that it contains an extra tuning parameter, i.e. it can be tuned in different ways to achieve finite-time convergence without overshoot. Therefore, it gives us more freedom to also reduce the higher-order harmonics generation, which is not possible with the PI+CI.

6. CONCLUSION

In this paper a novel GFORE-based PI-element is proposed which can overcome two limitations of a PCI-element. First, the proposed solution can prevent the limit cycle which is observed with a PCI. When properly tuned, the step response shows that it is possible to achieve finite-time convergence without any overshoot, which is not possible with a PCI or LTI PI-element. Second, the novel PI-element can reduce the generation of higher-order

harmonics, especially in the low-frequency range. Even though other alternative solutions exist that can achieve the same benefits, these either require trading off the beneficial phase-advantage at the open-loop crossover frequency, or they cannot be straightforwardly designed while taking the effect of higher-order harmonics into account. The reset-based PI-element proposed in this work does not face this trade-off. Instead, it can even improve the mentioned phase-advantage, or achieve the same phase-advantage with larger integral gain.

As a part of our future work, we will investigate how the proposed PI-element should be tuned in a closed-loop setting, e.g., to diminish higher-order harmonics generation. Furthermore, it is of interest to evaluate the behaviour of the novel element when controlling a more complex plant. For example, this concerns higher-order plants, and plants with a right-half plane zero or dead-time.

REFERENCES

Baños, A. and Vidal, A. (2007). Definition and tuning of a pi+ci reset controller. In *Proc. Eur. Control Conf. (ECC)*, 4792–4798.

Beker, O., Hollot, C., and Chait, Y. (2001). Plant with integrator: an example of reset control overcoming limitations of linear feedback. *IEEE Trans. Autom. Control*, 46(11), 1797–1799.

Clegg, J.C. (1958). A nonlinear integrator for servomechanisms. *Trans. Amer. Inst. Electr. Eng. II, Appl. Ind.*, 77(1), 41–42.

Freudenberg, J., Middleton, R., and Stefanpoulou, A. (2000). A survey of inherent design limitations. In *Proc. Amer. Control Conf. (ACC)*, volume 5, 2987–3001.

Guo, Y., Wang, Y., and Xie, L. (2009). Frequency-domain properties of reset systems with application in hard-disk-drive systems. *IEEE Trans. Control Syst. Technol.*, 17(6), 1446–1453.

Heertjes, M., Van Den Eijnden, S., Heemels, W., and Nijmeijer, H. (2021). A solution to gain loss in hybrid integrator-gain systems. In *Proc. IEEE Conf. Control Technol. Appl. (CCTA)*, 1179–1184.

Hosseini, S.A., Tavazoei, M.S., Van Eijk, L.F., and HosseinNia, S.H. (2022). Generalizing hybrid integrator-gain systems using fractional calculus. In *Proc. IEEE Conf. Control Technol. Appl. (CCTA)*, 1050–1055.

HosseinNia, S.H., Tejado, I., Torres, D., Vinagre, B.M., and Feliu, V. (2014). A general form for reset control including fractional order dynamics. *IFAC Proc. Vol.*, 47(3), 2028–2033.

Karbasizadeh, N. (2023). *Shaping Nonlinearity in Reset Control Systems to Realize Complex-Order Controllers: Application in Precision Motion Control*. Ph.D. thesis, Delft University of Technology.

Lamnabhi-Lagarrigue, F., Annaswamy, A., Engell, S., Isaksson, A., Khargonekar, P., Murray, R.M., Nijmeijer, H., Samad, T., Tilbury, D., and Van den Hof, P. (2017). Systems & control for the future of humanity, research agenda: Current and future roles, impact and grand challenges. *Annu. Rev. Control*, 43, 1–64.

Munnig Schmidt, R., Schitter, R., Rankers, A., and van Eijk, J. (2014). *The Design of High Performance Mechatronics: High-Tech Functionality by Multidisciplinary System Integration*. IOS Press, 2 edition.

Nair, U.R., Costa-Castelló, R., and Baños, A. (2018). Grid voltage regulation using a reset pi+ci controller for energy storage systems. *IFAC-PapersOnLine*, 51(4), 226–231.

Nuij, P., Bosgra, O., and Steinbuch, M. (2006). Higher-order sinusoidal input describing functions for the analysis of non-linear systems with harmonic responses. *Mech. Syst. Signal Process.*, 20(8), 1883–1904.

Saikumar, N., Heinen, K., and HosseinNia, S.H. (2021). Loop-shaping for reset control systems: A higher-order sinusoidal-input describing functions approach. *Control Eng. Pract.*, 111, 104808.

van Eijk, L.F., Beer, S., van Es, R.M.J., Kostić, D., and Nijmeijer, H. (2023). Frequency-domain properties of the hybrid integrator-gain system and its application as a nonlinear lag filter. *IEEE Trans. Control Syst. Technol.*, 31(2), 905–912.

Åström, K. and Hägglund, T. (2001). The future of pid control. *Control Eng. Pract.*, 9(11), 1163–1175.

Appendix A. CONSTRUCTION OF THE GFBI

The magnitude-characteristics of the LTI integrator in (9) are given by

$$|C_{\text{int}}(j\omega)| = \frac{1}{\omega}. \tag{A.1}$$

We can derive from (5) that the magnitude-characteristics for the SIDF of a GFbI are given by

$$|L_1(\omega)| = |H_1(\omega)||C_{\text{PI}}(j\omega)|. \tag{A.2}$$

We know from Lemma 1 that the magnitude-characteristics for the SIDF of a GFORE are given by

$$|H_1(\omega)| = \frac{\omega_{\text{r}}\sqrt{1+\Theta_{\text{D}}^2(\omega)}}{\sqrt{\omega_{\text{r}}^2+\omega^2}}, \tag{A.3}$$

while those of LTI element C_{PI} in (7) are

$$|C_{\text{PI}}(j\omega)| = \frac{\sqrt{\omega_{\text{c}}^2+\omega^2}}{\omega_{\text{c}}\omega}. \tag{A.4}$$

Finally, substituting (A.3)-(A.4) in (A.2) yields

$$|L_1(\omega)| = \frac{1}{\omega}\cdot\frac{\omega_{\text{r}}\sqrt{\omega_{\text{c}}^2+\omega^2}}{\omega_{\text{c}}\sqrt{\omega_{\text{r}}^2+\omega^2}}\cdot\sqrt{1+\Theta_{\text{D}}^2(\omega)}. \tag{A.5}$$

A.1 Low-frequent limit case

From Lemma 1 we conclude that $\Theta_{\text{D}}(0) = 0$. Then, utilizing (A.5), we find that $\lim_{\omega\to 0}|L_1(\omega)| = \lim_{\omega\to 0}\frac{1}{\omega}$. Therefore, the SIDF of the GFbI has equivalent magnitude-characteristics as the LTI integrator for the low-frequent limit case. Namely, from (A.1) it can be observed that $\lim_{\omega\to 0}|C_{\text{int}}(j\omega)| = \lim_{\omega\to 0}\frac{1}{\omega}$.

A.2 High-frequent limit case

We define $\Theta_{\text{D},\infty} := \lim_{\omega\to\infty}\Theta_{\text{D}}(\omega)$. From Lemma 1 we then conclude that $\Theta_{\text{D},\infty}$ is as in (8). Then, utilizing (A.5), we find that

$$\lim_{\omega\to\infty}|L_1(\omega)| = \lim_{\omega\to\infty}\frac{1}{\omega}\cdot\frac{\omega_{\text{r}}}{\omega_{\text{c}}}\cdot\sqrt{1+\Theta_{\text{D},\infty}^2}. \tag{A.6}$$

Next, substituting (8) in (A.6) results in $\lim_{\omega\to\infty}|L_1(\omega)| = \lim_{\omega\to\infty}\frac{1}{\omega}$. Therefore, the SIDF of the GFbI has equivalent magnitude-characteristics as the LTI integrator for the high-frequent limit case. Namely, from (A.1) it can be observed that $\lim_{\omega\to\infty}|C_{\text{int}}(j\omega)| = \lim_{\omega\to\infty}\frac{1}{\omega}$.